RSC Mechanochemistry

ROYAL SOCIETY OF CHEMISTRY

PAPER

View Article Online
View Journal | View Issue

Cite this: *RSC Mechanochem.*, 2024, **1**, 536

Exploring mass transfer as a parameter in mechanochemical processes†

Obida Bawadkji * and Rainer Haag

Mechanochemistry is increasingly recognized for its sustainability, environmental benefits, and efficiency in synthesizing a wide array of chemicals and materials. This research focuses on advancing our understanding of the factors that influence mechanochemical processes, which remains limited despite the broad application of these techniques in industry and research. Specifically, this paper explores the impact of mass transfer—a parameter previously underexplored in the context of mechanochemistry—on the outcome of chemical syntheses performed without solvents, thus avoiding the use of environmentally harmful substances and complex purification steps. This study introduces a novel multi-functional ball-mill medium design that enhances mass transfer, promotes more uniform kinetic energy distribution and material treatment, and increases overall synthesis efficiency. By analyzing the products of allotrope conversion, co-crystallization, and size reduction, we demonstrate how our new design enhances mechanochemical reactions. The findings indicate that adjusting the geometry of the milling media can significantly influence the chemical transformation processes. This advancement not only contributes to a deeper comprehension of mechanochemical synthesis but also opens avenues for more controlled and scalable production methods. The research underscores the importance of considering mass transfer in developing more effective mechanochemical technologies, paving the way for future innovations in this green chemistry field.

Received 25th April 2024
Accepted 12th September 2024

DOI: 10.1039/d4mr00041b

rsc.li/RSCMechanochem

Introduction

Mechanochemistry[1] has gained tremendous attention due to its sustainability, environmental friendliness, and outstanding efficiency as an advanced synthetic method for an ever-growing number of useful chemicals and materials.[2–5] Although currently applications of mechanochemistry are vast and cover many different important areas within industry and research, our understanding of the underlying processes which determine a mechanochemical procedure's outcome is limited.[4] A full comprehension of these parameters and their influence on process pathways is very much needed to further develop these advanced high-energy procedures, gain control of the outcomes, and scale product outputs.

Understanding these parameters can contribute towards the innovation of high-energy chemical synthesis as there are numerous variables which determine the outcome of mechanosynthesis as compared to simple milling/size reduction applications (*i.e.* as typically done for mineral research). Currently, there are two types of high-energy ball-milling devices: the high-energy planetary ball-mill and the vibrational-mill. Planetary ball-mills operate primarily through shear and impact forces, generated by the rotation of the milling jars as they orbit around a central axis, causing the milling media to collide with the material. Vibrational ball-mills, on the other hand, rely on the rapid oscillation of the milling chamber, inducing both impact and frictional forces that facilitate mechanochemical reactions. Outcomes from both devices mainly depend on the running time,[6,7] milling energy,[8–12] and milling atmosphere.[13] Research has focused on studying how these parameters affect mechanochemical syntheses[4] and some translated them to kinetic models.[14–16]

One crucial parameter for mechanochemical processes is 'mass transfer'. In a typical solvent-based procedure, mass transfer refers to the movement of reagents and other species within the solution, which is mainly determined by the choice of solvent and the mechanical agitation (*i.e.* stirring, shaking, *etc*…); Usually, a higher degree of solubility and stirring rate leads to more effective mass transfer, facilitating more efficient product formation. In a mechanochemical process, however, most chemical syntheses are "neat" reactions which do not require any solvent. This eliminates the use of environmentally hazardous agents and costly concentration as well as purification steps.[1] The mixing of materials inside a ball-mill chamber is achieved by the movement of the chamber and the milling medium. The mass transfer in this context depends on the movement kinetics of the ball-mill chamber and milling

Institut für Chemie und Biochemie, Freie Universität Berlin, Takustr. 3, 14195 Berlin, Germany. E-mail: obida.bawadkji@fu-berlin.de

† Electronic supplementary information (ESI) available. See DOI: https://doi.org/10.1039/d4mr00041b

medium. This is influenced by the ball-mill chamber volume, filling ratio, size and weight of the milling medium, and the ball-mill's operating parameters, such as the rounds-per-minute for a planetary ball-mill (rpm) or oscillation frequency of a vibrational milling device.

For milling and size reduction applications, conventional parameters are generally known for optimal output. For mechanochemical syntheses, on the other hand, the parameters need to be carefully optimized to obtain an optimal outcome.[4,17] In these cases, the milling energy, milling time, reaction atmosphere, pressure, the material of the ball-mill chamber and medium, as well as the consistency/texture of the reactants have a great influence on the chemical process, and research has elucidated how these parameters influence certain chemical transformations.[4,17,18]

Despite the importance of these factors, there are no reports on the degree of mass transfer as a parameter and its influence on mechanosynthesis. In this work, we study how chemical processes are affected by the degree of mass transfer by analysis of products from three different types of energy demanding procedures, namely allotrope conversion, co-crystallization, and size reduction. From this, we propose a novel geometry for the ball-mill medium which serves three functions: homogenization of reagents inside the ball-mill chamber during the milling process, higher kinetic energy transfer, and uniform distribution of the kinetic energy output, altogether leading to more efficient product formation.

In this work, a novel multi-functional design to ball-mill media is presented which prompts efficient mass transfer and generates uniformly distributed and higher energy transfer within a mechanochemical process, granting much greater control and efficiency in product formation.

Results & discussion

Modified ball-mill medium design

The design of the novel modified ball-mill medium (MB) as compared to normal ball-mill medium (NB) can be simply described as a 3 × 3 corrugation on the outer surface of the balls (Fig. 1). In this study, we used standard 10 mm stainless-steel balls supplied by FRITSCH GmbH, and modified them with 1 mm deep corrugations (or 20% of the radius) from the surface of the balls (see ESI† for detailed production method). The same modification can be applied to balls of different sizes and materials (tungsten carbide, ceramic, *etc*…). Similar results can be expected with different shapes and number of carved corrugations. The concept of the design is to increase the number of contact points per ball to allow for more efficient transfer of kinetic energy, with set spacings in between that mix and homogenize particulate matter for more efficient mass transfer, and an overall spherical shape to preserve the general motion of the milling medium inside the PBM, all together resulting in more efficient material treatment. Abrasion analysis of the MB milling medium was tested by weighing the medium before and after 8 hours of milling at 600 rpm, indicating little abrasion after prolonged milling (ESI 1†).

Co-crystallization of nicotinamide and salicylic acid

Co-crystal drug formulations are gaining increased attention and are expected to continue acquiring significance as they allow facile and effective ways of modifying chemical and physical properties of important active pharmaceutical ingredients (APIs).[19,20] The co-crystallization of nicotinamide (Nic) and salicylic acid (Sal), both of which are popular APIs, can be achieved mechanochemically and has been previously used as a control reaction to study mechanochemical processes *via* Raman spectroscopy.[21,22] This can be done by observing Raman band intensity changes associated both with the formation of the hydrogen-bonded co-crystal (NicSal) and the disruption of the Nic and Sal crystal structures. Specifically, Raman bands within the 30–200 cm^{-1} spectral range, which are associated to lattice vibrations of whole crystal structures, are mostly affected by crystal structure rearrangements, and this allows us to monitor such reactions closely (Fig. 2b, c and ESI 2†).[22,23] Moreover, depletion of the characteristic bands corresponding to Nic at 1042 cm^{-1} and Sal at 778, 1324, and 1636 cm^{-1} and the evolution of the band at 795 cm^{-1} corresponding to the formed NicSal co-crystal can be monitored to track the reaction process (Fig. 2b and c).

To study the influence MB, several co-crystallization monitoring reactions were performed and studied mainly *via* Raman spectroscopy. A 1 : 1 molar ratio of Nic and Sal were combined in a planetary ball-mill chamber together with either MB or NB (25 : 1 ball-to-powder ratio w/w, or BPR). The chamber was sealed and placed in its respective PBM, which operated at 600 rpm for a total of 60 min with a sample extracted for analysis after every 10 min (Fig. 2a). As shown in Fig. 2c,

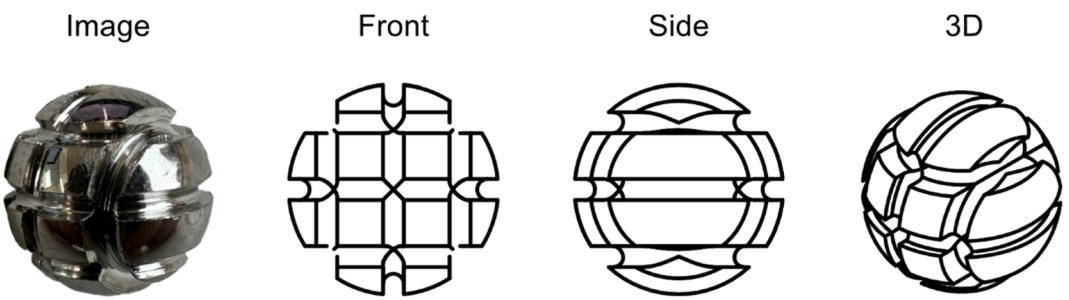

Fig. 1 Image and technical drawings of the proposed modified geometry for the ball-mill medium (MB).

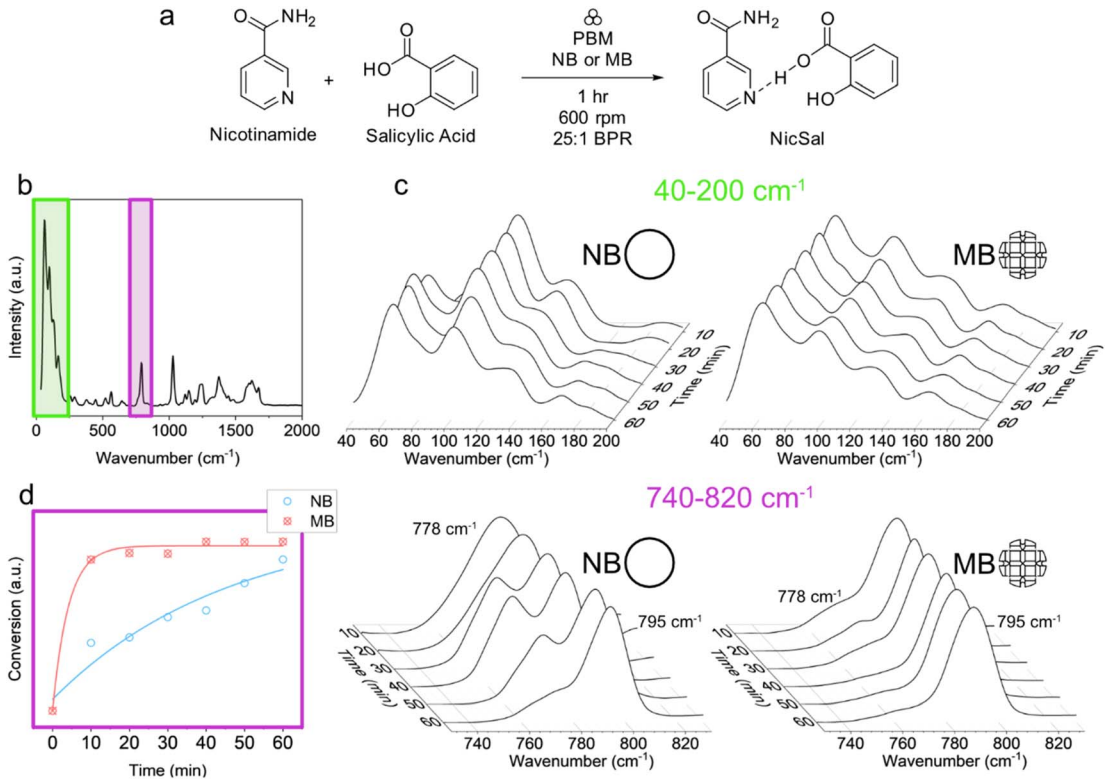

Fig. 2 (a) Scheme of the co-crystallization of Nic and Sal to form NicSal. (b) Raman spectrum of NicSal. (c) Raman spectra from a monitored synthesis of NicSal produced *via* PBM using either NB or MB. (d) Co-crystallization conversion of NicSal *via* PBM using NB or MB determined by eqn (1).

evolution of the NicSal co-crystal using MB is evidenced after only 10 min of PBM, whereas the evolution of a similar amount of the NicSal co-crystal using NB can only be observed after 60 min of PBM; the spectral profile within the phonon region of 30–200 cm^{-1} corresponding to the NicSal co-crystal is present after 10 min of PBM using MB, whereas a similar spectral profile using NB appears only after 60 min of PBM (Fig. 2c). This is directly correlated to the evolution profiles of the characteristic NicSal co-crystal Raman vibrational band at 795 cm^{-1} for MB and NB. A semiquantitative analysis can be obtained by plotting the intensity ratios (as arbitrary units, or a.u.) of the evolving Raman band corresponding to NicSal at 795 cm^{-1} (I_{795}) against the depleting Raman band corresponding to Sal at 778 cm^{-1} (I_{778}) following eqn (1) (Fig. 2d):

$$\text{Conversion(a.u.)} = \frac{I_{795}}{(I_{778} + I_{795})} \quad (1)$$

The efficient conversion performance of MB as compared to NB is clearly indicated by observing the determined reaction conversion profile.

Allotrope conversion from red to black phosphorus

Black phosphorus nanomaterials have been attracting great attention recently as they are distinguished with unique features fitting for a wide range of applications.[24–30] The allotropic transformation from red to black phosphorus is an energy-demanding process which can also be achieved mechanochemically and can be easily monitored using Raman spectroscopy since the spectral profiles of the two allotropes are distinctive.[16,31–35] This can be done mainly by tracking changes in the Raman spectral profiles, specifically the depletion of broad vibrational bands corresponding to red phosphorus between ~368–425 cm^{-1}, the blue shift of the B_1 red phosphorus peak at ~350 cm^{-1} to the A_g^1 black phosphorus peak at ~360 cm^{-1}, and the evolution of the B_{2g} and the A_g^2 black phosphorus peaks at 435 cm^{-1} and 463 cm^{-1}, respectively. Additionally, visual observation of the color change of the reaction product from red to black could give a simple indication of the mechanochemical conversion.

The influence of MB as compared to NB for mechanochemical allotropic transformation reactions was investigated using this conversion as a model reaction. Here, the simultaneous homogenization property of MB was investigated by using a ratio of 1 : 4 MB-to-NB to eliminate the 'mechanical shielding' phenomenon. In this context, mechanical shielding occurs when outer layers of powder absorb most of the mechanical energy, preventing inner layers from receiving adequate impact or shear forces. As a result, only the surface layers undergo the desired mechanochemical reactions, while the material beneath remains largely untreated, leading to inefficient reactions and inconsistent product quality. Therefore, the role of MB units is to homogenize the powder in the ball-mill chamber so that the entirety of the red phosphorus is

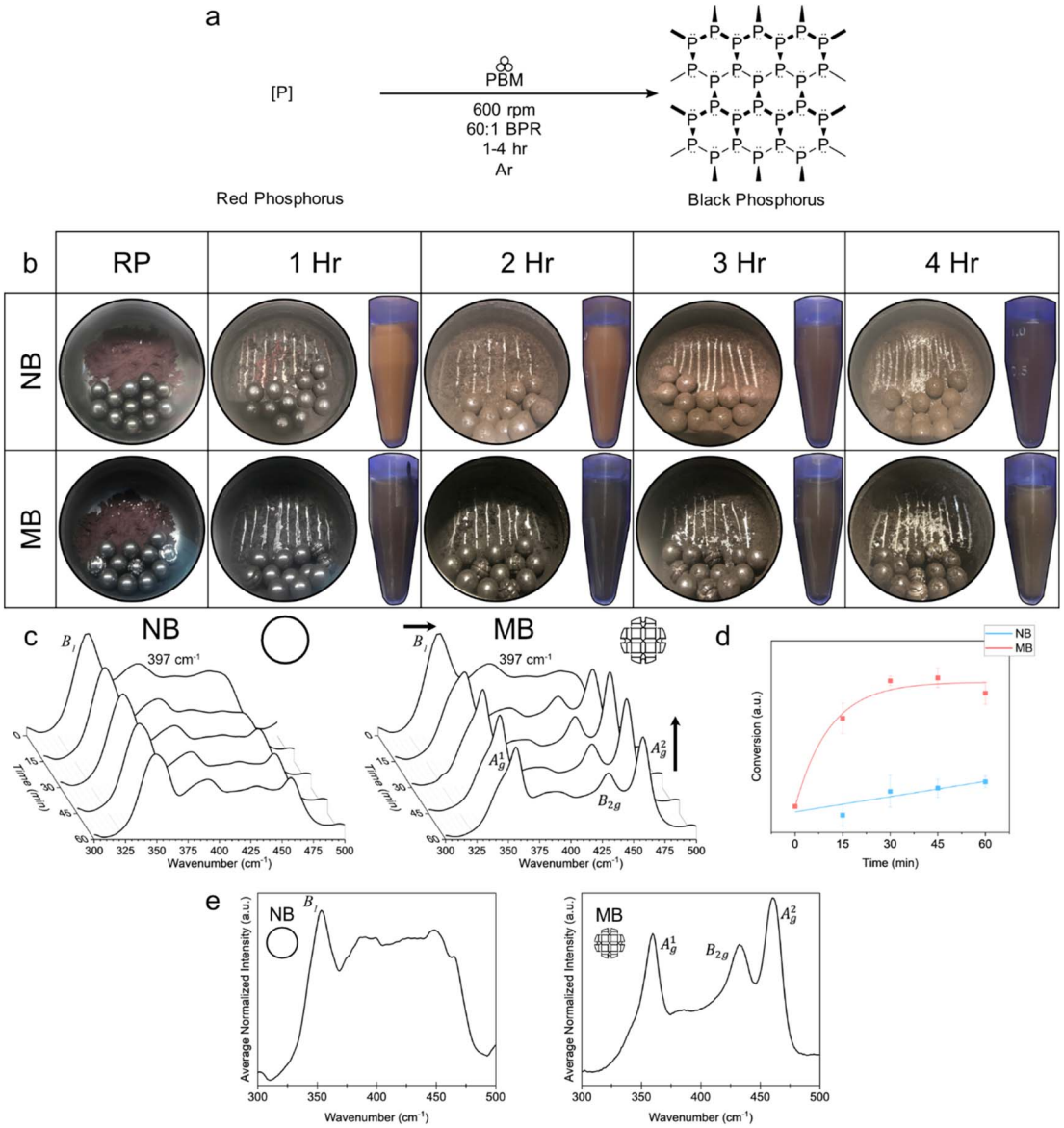

Fig. 3 (a) Allotrope conversion of RP to BP *via* PBM using NB or MB. (b) Images of the ball-mill chamber before and after PBM using NB or MB with carvings along with images of 1 mg mL^{-1} dispersions of the samples. (c) Raman spectra of collected samples after PBM using NB or MB at different time points. (d) Allotrope conversion to black phosphorus *via* PBM using NB or MB determined by eqn (2). (e) Raman analysis of samples obtained from red to black phosphorus mechanochemical allotropic conversion using either only NB or MB.

receiving adequate mechanochemical treatment. To test this, red phosphorus was sealed together with either a mixture of MB and NB or only NB (60 : 1 BPR) in a planetary ball-mill chamber under argon (to prevent degradation of black phosphorus) and was treated by PBM at 600 rpm, with samples extracted throughout the process to track the allotropic transformation (Fig. 3a).

Raman spectrum of the formed BP using MB indicates an effective allotropic conversion as seen mainly by the pronounced evolution of the B_{2g} and the $A_g{}^2$ black phosphorus vibrational peaks at 435 cm^{-1} and 463 cm^{-1}, respectively (Fig. 3c and ESI 3†). Comparatively, these vibrational bands from using NB do not significantly evolve. Moreover, using MB results in the strong depletion of the broad band between 368–425 cm^{-1} and the blue shift of the B_1 red phosphorus peak at 350 cm^{-1} to the $A_g{}^1$ black phosphorus peak at ~360 cm^{-1}, all of which are not clearly indicated by the analysis of the formed BP using only NB. A semiquantitative analysis can be obtained by plotting the intensity ratios (in a.u.) of the evolving Raman band corresponding to the $A_g{}^2$ black phosphorus vibrational peak at 463 cm^{-1} (I_{463}) against the depleting Raman band corresponding to red phosphorus at 397 cm^{-1} (I_{397}) following eqn (2) (Fig. 3d):

$$\text{Conversion(a.u.)} = \frac{I_{463}}{(I_{463} + I_{397})} \quad (2)$$

The successful allotropic conversion when using MB can be attributed to the continuous mixing during the milling process

which eliminates the mechanical shielding phenomenon. Regarding the red-to-black phosphorus allotropic conversion using only NB, one can observe this phenomenon by revealing the red layer of the powder trapped between the outer surface exposed to the milling medium and the ball-mill chamber itself, indicating the presence of untreated RP powder. As seen in Fig. 3b, using NB leads to an abundant amount of unconverted red phosphorus indicated by carving lines into the milled particles to uncover the solid material beneath the surface. Using MB, on the other hand, leaves almost no trace of red phosphorus seen visually, indicating successful continuous homogenization of the solid matter during the milling process and preventing mechanical shielding, leading to a higher quality product that can be obtained in a shorter time (Fig. 3b). 1 mg mL^{-1} dispersions of the powder in isopropanol further indicate the stark difference in quality of the treated powders by observation of the color.

Altogether, the characterizations reflect the advantages of the corrugated design of MB, which is suitable for mixing particulate matter. The ridges on the surface of MB allow for an effective penetration into particulate matter. This design ensures that the ball-mill medium can practically mix the particles throughout its depth, resulting in more uniform mixing. This also leads to the breaking up of formed clumps which prevents agglomeration and results in a homogeneous mass transfer of reactants inside the ball-mill chamber. On the other hand, the smooth surface of NB prevents the deep penetration and would slip and slide on the surface of the particles, leading to mechanical shielding and uneven mixing as particulate solid would not be reached by the medium. This causes non-uniform mass transfer of particles inside ball-mill chambers which limits the ability for PBM being an efficient alternative to costly and non-environmentally friendly solvent-based procedures.[36–38] This issue becomes particularly significant when considering the upscaling of mechanochemical reactions. High material loading in the ball-mill chamber or a low BPR reduces the mechanical treatment of the sample compared to processes with low material loading or a high BPR. For instance, red phosphorus powder treated with a 25 : 1 BPR using either NB or MB (6 units each) results in products with markedly different degrees of allotropic conversion (Fig. 3e) after milling at 600 rpm for 4 hours. This difference can be visualized by examining the Raman spectral profiles obtained from the products. The Raman maps from NB-treated red phosphorus powder reveal significantly less allotropic conversion overall compared to the Raman spectral profiles from MB-treated samples, which clearly indicate the formation of black phosphorus.

In this case, the advantage of using MB as a homogenizing agent is highlighted. Typically, a small amount of liquid can be added as a dispersing agent to the reaction mixture. However, the main disadvantage of adding additional substances is the

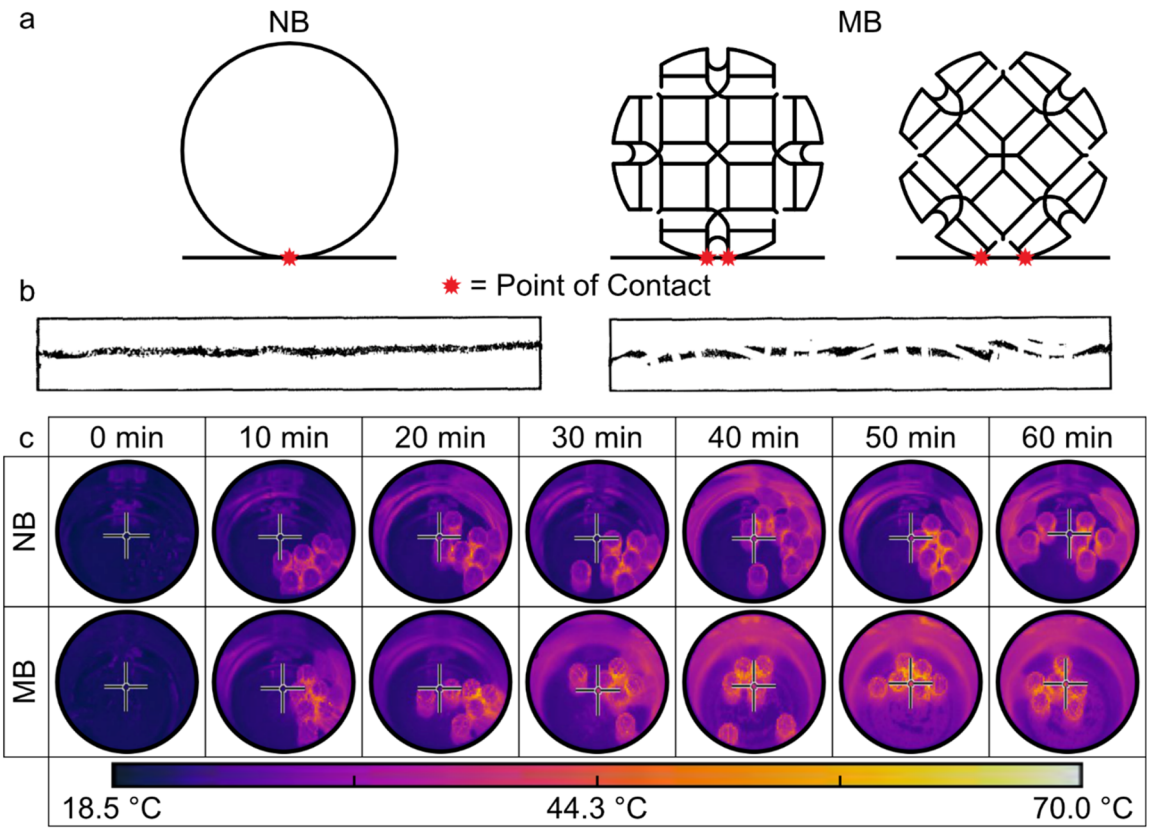

Fig. 4 (a) Possible points of contact/mechanical treatment at a given instance for both NB and MB. (b) Ink prints on paper using NB and MB showing the difference of the distribution of ball contact points. (c) Thermal images of ball-mill chamber and NB or MB after PBM captured using a FLIR camera.

introduction of contaminants which can alter the properties of the produced nanomaterials. Moreover, the purification of these nanomaterials from such agents is costly and time-demanding, especially for high-boiling point solvents.[4,39]

Another factor contributing to the higher conversion is the higher transfer of kinetic energy that is generated by MB in comparison to NB. The higher transfer of energy is attributed to more frequent contact MB produces with the inner surface of the ball-mill chamber during the milling process, which is owed to the corrugated design on the spherical surface. The number of contact points at an instance is determined by the orientation of the MB on the inner surface of the ball-mill chamber (Fig. 4a). To visualize this, MB was covered with ink and controllably rolled on a straight line on a sheet of paper (analogous to a 'footprint test' for tire designers) showing the greater distribution of contact points MB covers (Fig. 4b).

The greater number of contact points generated by MB leads to more shearing and friction inside the ball-mill chamber during the milling procedure, which results in a greater distribution and amount of kinetic energy output as compared to NB. Without the presence of materials inside the chamber, the kinetic energy is dissipated into the ball-mill chamber in the form of heat. One way to visualize this is to capture thermal images of the ball-mill chamber after milling for a certain amount of time. Using a forward looking infrared (FLIR) camera, the temperature of the ball-mill chamber after 10 min intervals of milling at 600 rpm using 6 balls of either MB or NB was recorded (Fig. 4c), as well as after 10 min of milling at different rpm (200–600 rpm for 10 min, ESI 4†). Clearly, the greater transfer of kinetic energy produced by MB led to an increase in the average temperature of the ball-mill chamber as compared to NB. More importantly, however, is the noticeable greater distribution of the kinetic energy generated by MB. The higher number of contact points of MB distributes the kinetic energy over a larger area within the ball-mill chamber as compared to NB, creating a homogeneous environment for chemical conversions resulting in higher quality products produced more efficiently. Moreover, the irregular shape of the MB can induce irregular motion of the milling medium within the ball-mill chamber. The ridges on the MB's surface cause deflections in random directions upon collision with other units, resulting in a chaotic motion. This randomness in movement generates shearing and impacts across diverse areas of the ball-mill chamber, thereby ensuring a more homogeneous treatment of the materials inside, as seen by the temperature profile of the central basal part of the ball-mill chamber treated with MB in comparison to NB (Fig. 4c).

Particle size reduction of titanium dioxide

Surely, with such features, MB is expected to not only reduce particle sizes more rapidly, but also achieve greater monodispersity of the particle sizes more efficiently. To test this, titanium dioxide (TiO_2), a commonly milled substance, was treated with 6 units of MB or 6 of NB over 15 min at 600 rpm.

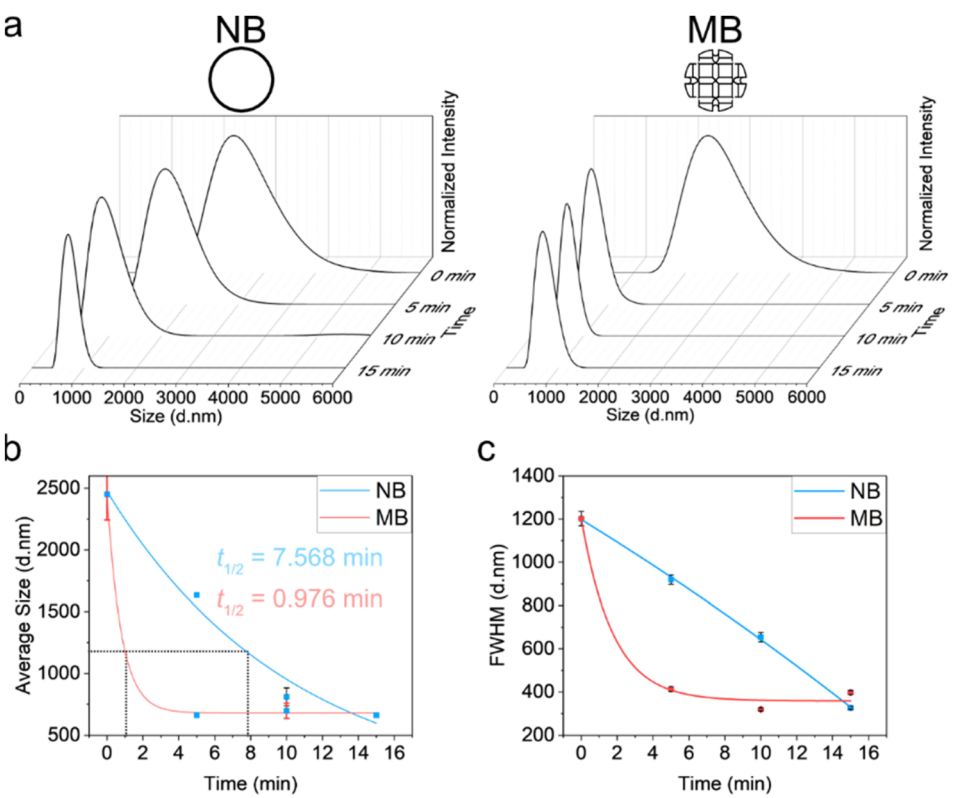

Fig. 5 (a) DLS of TiO_2 treated with PBM using NB or MB. (b) Average size of milled particles derived from DLS data. (c) FWHM analysis derived from average particle size distribution of milled nanoparticles.

Samples were extracted every 5 min and analyzed *via* dynamic light scattering (DLS, Fig. 5a). As indicated in Fig. 5b, MB was able to reduce the average particle size of TiO_2 to ~660 nm in hydrodynamic diameter within 5 min of milling, whereas NB achieved the same only after 15 min of milling. Additionally, the full-width at half-maximum analysis derived from the average particle size distributions of the milled particles indicate that MB is able to efficiently achieve more monodisperse size distributions in comparison to NB (Fig. 5c).

Conclusion

In this work, we highlight the importance of mass transfer during solvent-less mechanochemical procedures. To do this, a novel corrugated geometry of the ball-mill medium is presented and investigated, which was shown to be capable of effective simultaneous homogenization of materials undergoing PBM leading to more uniform treatment of samples, as well as delivering higher and uniformly distributed kinetic energies when high energy treatment is needed.

Data availability

All data generated or analyzed during this study are included in this article and its ESI† file.

Conflicts of interest

There are no conflicts of interest to declare.

Acknowledgements

The authors would like to thank Frank Totzauer from the BCP Department Workshop of the Freie Universität Berlin for his support on the production of MB. The authors would also like to acknowledge the support of the Freie Universität Berlin, Bio-SupraMol, as well as the Deutsche Forschungsgemeinschaft (DFG, German Research Foundation) – Project ID 431232613 – SFB 1449.

References

1 J. J. Gilman, *Science*, 1996, **274**, 65.
2 S. L. James, C. J. Adams, C. Bolm, D. Braga, P. Collier, T. Friščić, F. Grepioni, K. D. M. Harris, G. Hyett, W. Jones, A. Krebs, J. Mack, L. Maini, A. G. Orpen, I. P. Parkin, W. C. Shearouse, J. W. Steed and D. C. Waddell, *Chem. Soc. Rev.*, 2012, **41**, 413–447.
3 J.-L. Do and T. Friščić, *ACS Cent. Sci.*, 2017, **3**, 13–19.
4 S. Mateti, M. Mathesh, Z. Liu, T. Tao, T. Ramireddy, A. M. Glushenkov, W. Yang and Y. I. Chen, *Chem. Commun.*, 2021, **57**, 1080–1092.
5 A. Krusenbaum, S. Grätz, G. T. Tigineh, L. Borchardt and J. G. Kim, *Chem. Soc. Rev.*, 2022, **51**, 2873–2905.
6 Y. Chen and J. S. Williams, *J. Alloys Compd.*, 1995, **217**, 181–184.
7 Y. Chen, Z. L. Li and J. S. Williams, *J. Mater. Sci. Lett.*, 1995, **14**, 542–544.
8 L. H. Li, Y. Chen, G. Behan, H. Zhang, M. Petravic and A. M. Glushenkov, *J. Mater. Chem.*, 2011, **21**, 11862.
9 T. Tao, A. M. Glushenkov, H. Hu, Q. Chen and Y. Chen, *J. Alloys Compd.*, 2010, **504**, S315–S318.
10 Y. Chen, J. Fitz Gerald, J. S. Williams and S. Bulcock, *Chem. Phys. Lett.*, 1999, **299**, 260–264.
11 H. Kulla, S. Haferkamp, I. Akhmetova, M. Röllig, C. Maierhofer, K. Rademann and F. Emmerling, *Angew. Chem., Int. Ed.*, 2018, **57**, 5930–5933.
12 H. Kulla, M. Wilke, F. Fischer, M. Röllig, C. Maierhofer and F. Emmerling, *Chem. Commun.*, 2017, **53**, 1664–1667.
13 T. Xing, S. Mateti, L. H. Li, F. Ma, A. Du, Y. Gogotsi and Y. Chen, *Sci. Rep.*, 2016, **6**, 35532.
14 F. Delogu, G. Mulas, L. Schiffini and G. Cocco, *Mater. Sci. Eng. A*, 2004, **382**, 280–287.
15 J. Blázquez, A. Manchón-Gordón, J. Ipus, C. Conde and A. Conde, *Metals*, 2018, **8**, 450.
16 S. V. Pedersen, F. Muramutsa, J. D. Wood, C. Husko, D. Estrada and B. J. Jaques, *npj 2D Mater. Appl.*, 2020, **4**, 36.
17 J. L. Howard, Q. Cao and D. L. Browne, *Chem. Sci.*, 2018, **9**, 3080–3094.
18 V. A. Volkov, I. A. El'kin, A. V. Zagainov, A. V. Protasov and E. P. Elsukov, *Phys. Met. Metallogr.*, 2014, **115**, 557–565.
19 D. J. Good and N. Rodríguez-Hornedo, *Cryst. Growth Des.*, 2009, **9**, 2252–2264.
20 A. Trask, W. Motherwell and W. Jones, *Int. J. Pharm.*, 2006, **320**, 114–123.
21 D. J. Berry, C. C. Seaton, W. Clegg, R. W. Harrington, S. J. Coles, P. N. Horton, M. B. Hursthouse, R. Storey, W. Jones, T. Friščić and N. Blagden, *Cryst. Growth Des.*, 2008, **8**, 1697–1712.
22 S. Lukin, K. Užarević and I. Halasz, *Nat. Protoc.*, 2021, **16**, 3492–3521.
23 T. Stolar, S. Lukin, M. Tireli, I. Sović, B. Karadeniz, I. Kereković, G. Matijašić, M. Gretić, Z. Katančić, I. Dejanović, M. D. Michiel, I. Halasz and K. Užarević, *ACS Sustainable Chem. Eng.*, 2019, **7**, 7102–7110.
24 D. An, J. Fu, Z. Xie, C. Xing, B. Zhang, B. Wang and M. Qiu, *J. Mater. Chem. B*, 2020, **8**, 7076–7120.
25 Y. Zhang, C. Ma, J. Xie, H. Ågren and H. Zhang, *Adv. Mater.*, 2021, **33**, 2100113.
26 P. Li, J. Lu, H. Cui, S. Ruan and Y.-J. Zeng, *Mater. Adv.*, 2021, **2**, 2483–2509.
27 O. Bawadkji, M. Cherri, A. Schäfer, S. Herziger, P. Nickl, K. Achazi, I. S. Donskyi, M. Adeli and R. Haag, *Adv. Mater. Inter.*, 2022, 2201245.
28 S. Anju, J. Ashtami and P. V. Mohanan, *Mater. Sci. Eng. C*, 2019, **97**, 978–993.
29 J. R. Choi, K. W. Yong, J. Y. Choi, A. Nilghaz, Y. Lin, J. Xu and X. Lu, *Theranostics*, 2018, **8**, 1005–1026.
30 Z. Guo, H. Zhang, S. Lu, Z. Wang, S. Tang, J. Shao, Z. Sun, H. Xie, H. Wang, X.-F. Yu and P. K. Chu, *Adv. Funct. Mater.*, 2015, **25**, 6996–7002.
31 Y. Akahama, M. Kobayashi and H. Kawamura, *Solid State Commun.*, 1997, **104**, 311–315.

32 C.-M. Park and H.-J. Sohn, *Adv. Mater.*, 2007, **19**, 2465–2468.
33 C. Ferrara, E. Vigo, B. Albini, P. Galinetto, C. Milanese, C. Tealdi, E. Quartarone, S. Passerini and P. Mustarelli, *ACS Appl. Energy Mater.*, 2019, **2**, 2794–2802.
34 C. Sun, L. Wen, J. Zeng, Y. Wang, Q. Sun, L. Deng, C. Zhao and Z. Li, *Biomaterials*, 2016, **91**, 81–89.
35 M. Zhao, H. Qian, X. Niu, W. Wang, L. Guan, J. Sha and Y. Wang, *Cryst. Growth Des.*, 2016, **16**, 1096–1103.
36 St. Palzer, *Powder Technol.*, 2011, **206**, 2–17.
37 Z. Wu, Y. Liang, E. Fu, J. Du, P. Wang, Y. Fan and Y. Zhao, *Metals*, 2018, **8**, 281.
38 O. Williams, C. Eastwick, S. Kingman, D. Giddings, S. Lormor and E. Lester, *Ind. Crops Prod.*, 2017, **101**, 92–102.
39 C. Lin, L. Yang, L. Ouyang, J. Liu, H. Wang and M. Zhu, *J. Alloys Compd.*, 2017, **728**, 578–584.